

Quantum Anomalous Hall Effect in Antiferromagnetism

Peng-Jie Guo,^{1,*} Zheng-Xin Liu,^{1,†} and Zhong-Yi Lu^{1,‡}

¹*Department of Physics and Beijing Key Laboratory of Opto-electronic Functional Materials & Micro-nano Devices, Renmin University of China, Beijing 100872, China*

(Dated: May 16, 2022)

So far, experimentally realized quantum anomalous Hall (QAH) insulators all exhibit ferromagnetic order and the QAH effect only occurs at very low temperatures; Conceptually, the QAH effect is based on ferromagnetism or staggered flux. On the other hand, up to now the QAH effect in antiferromagnetic (AFM) systems has never been reported. In this letter, we realize the QAH effect by proposing a four-band lattice model with static AFM order, which indicates the QAH effect can be found in AFM materials with low lattice symmetry. Then, as a prototype, we demonstrate that a monolayer CrO can be switched from an AFM Weyl semimetal to an AFM QAH insulator by applying strain to lower its symmetry, based on theoretical analysis and the first-principles electronic structure calculations. Our work not only proposes a new scenario to search for QAH insulators, but also reveals a way to considerably increase the critical temperature of the QAH phase.

Introduction. Anomalous Hall effect, which exists in ferromagnetic metals[1, 2], means that the electric Hall conductance remains to be finite even at zero external magnetic field. Furthermore, if the system becomes insulating, the Hall conductance is quantized to an integer C times e^2/h with C being the Chern number of its band structure. This effect is called the quantum anomalous Hall (QAH) effect. QAH insulators, i.e. magnetic insulators exhibiting QAH effect ($C \neq 0$), as important members in the family of quantum Hall systems, have attracted intensive interest from both theoretical and experimental physicists [3–8]. In 1988, Haldane proposed a lattice model of spinless fermions to realize integer Hall effect in a staggered magnetic flux with zero net magnetic field[9]. Later it was proposed that ferromagnetic insulators with spin-orbit coupling (SOC) may exhibit QAH effect [4, 10]. Meanwhile, many materials have been predicted to be QAH insulators[11–25]. So far, QAH effect has been experimentally observed in four different classes of two-dimensional (2D) systems: thin films of magnetically doped topological insulators[26], thin films of the intrinsic magnetic topological insulators[27], moiré materials formed from graphene[28], and transition metal dichalcogenides[29]. In all of these materials, the QAH plateau only shows up at very low temperatures (of order of 1 Kelvin or lower).

It was believed that ferromagnetism is necessary for experimental realization of QAH effect[4]. However, ferromagnetism can be found easily in metals but rarely in insulators. For this reason, the critical temperature of the QAH phase is very low. On the other hand, there are plenty of AFM insulating materials in nature even above room temperatures. However, so far the QAH effect has never been found in AFM systems, even the corresponding mechanism has never been proposed. Supposing QAH effect can be realized in AFM insulators (especially those containing collinear AFM order), then the realization of QAH effect will be much cheaper. Attractively, the critical temperature for observing the QAH

effect may be greatly increased since the critical temperature of the AFM order can be very high. The resultant AFM QAH insulators can have extensive applications in designing devices. Therefore, the realization of QAH effect in AFM materials is a very important issue both academically and practically.

Collinear antiferromagnetic (AFM) systems usually possess an ‘effective time-reversal’ symmetry such as $\{\mathcal{T}|\tau\}$ or \mathcal{IT} , where \mathcal{T} stands for the time reversal operation, τ denotes the associated fractional translation, and \mathcal{I} represents the spatial inversion. Such an ‘effective time-reversal’ symmetry restricts the Chern number of a gapped ground state to be $C = 0$, resulting in a trivial band insulator. This limits the study of QAH effect in collinear AFM systems. However, not all collinear AFM systems have the ‘effective time-reversal’ symmetry. Exceptions include the systems having type-I or some of the type-III magnetic space groups. QAH effect can be possibly realized in these collinear AFM insulators.

In this letter, we propose a four-band lattice model to realize QAH effect in a collinear AFM insulator. Furthermore, based on symmetry analysis and the first-principles electronic structure calculations, we illustrate that a monolayer CrO is a collinear AFM semimetal with C_{2v} symmetry protected Weyl cones robust against SOC. And we further show that by applying external strain to lower its point group symmetry, the monolayer CrO can open a gap and be turned into an AFM QAH insulator.

Lattice model. We consider a lattice with two sites (labeled by sublattice index $\alpha = 1, 2$) in each unit cell which contains anti-parallel magnetic moments $\mathbf{m}_1 = -\mathbf{m}_2 = \mathbf{m}$. The tight-binding model for spin-orbit coupled elec-

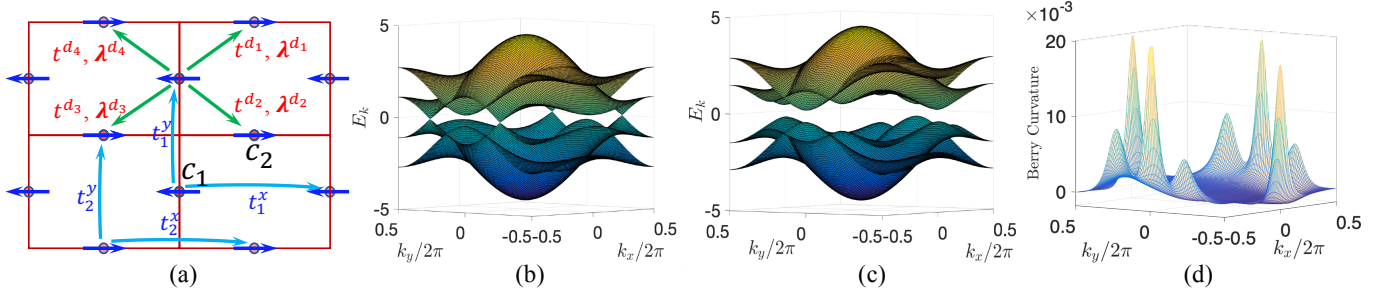


FIG. 1. Model for the AFM QAH insulator. (a) illustration of the Hamiltonian in Eq. (1); (b) without SOC the ground state being a Weyl semimetal with a pair of Weyl cones on the (π, k_y) boundary of the BZ; (c) with SOC the band structure being gapped with Chern number $C = 1$; (d) the Berry curvature calculated from the unitary transformed Hamiltonian with $\mathbf{d}_i \rightarrow \mathbf{d}_i - \frac{1}{2}(\mathbf{x} + \mathbf{y})$.

trons in the lattice reads

$$\begin{aligned}
 H = & \sum_{j, d_i} \left[t^{d_i} C_{1,j}^\dagger C_{2,j+\mathbf{d}_i} + C_{1,j}^\dagger (i\lambda^{d_i} \cdot \boldsymbol{\sigma}) C_{2,j+\mathbf{d}_i} + \text{h.c.} \right] \\
 & + \sum_{\alpha, j} \left[t_\alpha^x C_{\alpha, j}^\dagger C_{\alpha, j+\mathbf{x}} + t_\alpha^y C_{\alpha, j}^\dagger C_{\alpha, j+\mathbf{y}} + \text{h.c.} \right] \\
 & + \sum_{\alpha, j} C_{\alpha, j}^\dagger [\mu_\alpha \sigma_0 + \mathbf{m}_\alpha \cdot \boldsymbol{\sigma}] C_{\alpha, j}, \quad (1)
 \end{aligned}$$

where $C_{\alpha, j}^\dagger = (c_{\alpha, j\uparrow}^\dagger, c_{\alpha, j\downarrow}^\dagger)$ are electron creation operators, t^{d_i} and t_α^x, t_α^y are the kinetic hopping terms along $\mathbf{d}_{1,2,3,4}$ and \mathbf{x}, \mathbf{y} directions respectively, with $\mathbf{x} = a_1 \hat{x}$, $\mathbf{y} = a_2 \hat{y}$, a_1, a_2 being the lattice constants and \hat{x}, \hat{y} being unit vectors, and $\mathbf{d}_{1,3} = \pm \frac{1}{2}(\mathbf{x} + \mathbf{y})$, $\mathbf{d}_{2,4} = \pm \frac{1}{2}(\mathbf{x} - \mathbf{y})$. The $i\lambda^{d_i} \cdot \boldsymbol{\sigma}$ term denotes spin-orbit coupling, $\mathbf{m}_\alpha = (-1)^\alpha \mathbf{m}$ stands for the static collinear AFM order which couples to the electron spin as a Zeeman field, and μ_α represents the chemical potential on the α -sublattice. We further define $\mu_\pm = \frac{1}{2}(\mu_1 \pm \mu_2)$, where μ_- is the staggered potential energy and μ_+ is adopted such that the energy bands are half-filled. Here we ignore the correlation between the electrons by simply assuming that the AFM moment couples to the electron spin as a Zeeman field. The effect of electron correlations, such as the Anderson or the Kondo coupling terms, will be left for future study.

Since inversion symmetry is crucial to guarantee a nonzero Chern number, it requires that $t^{d_1} = t^{d_3}$, $t^{d_2} = t^{d_4}$ and $\lambda^{d_1} = \lambda^{d_3}$, $\lambda^{d_2} = \lambda^{d_4}$. For simplicity, we set $t^{d_1} = t^{d_2} = t^d$ and $\lambda^{d_1} = -\lambda^{d_2} = \boldsymbol{\lambda}$. Furthermore, to ensure that the energy bands have a full gap, we let $t_\alpha^m = (-1)^\alpha t^m$ with $m = x, y$. If $\mathbf{m} \cdot \hat{z} = \boldsymbol{\lambda} \cdot \hat{z} = 0$, then the spin-orbit coupled point symmetries of the Hamiltonian (1) form a magnetic point group $2'/m' = \{E, \mathcal{I}, \mathcal{T}C_2^z, \mathcal{T}M_z\}$. Specially, the symmetry is enhanced if $\boldsymbol{\lambda} \cdot \mathbf{m} = 0$. For example, when $\boldsymbol{\lambda} \parallel \hat{y}$ and $\mathbf{m} \parallel \hat{x}$, then the enhanced symmetry group generated by $\mathcal{T}C_2^z, \mathcal{T}M_z$ and M_x reads $2'/m'm = \{E, \mathcal{I}, C_2^x, M_x, \mathcal{T}C_2^z, \mathcal{T}M_z, \mathcal{T}C_2^y, \mathcal{T}M_y\}$.

After the Fourier transformation, the above Hamilto-

nian can be rewritten in momentum space as

$$H = \sum_k (C_{1k}^\dagger \Gamma_k^{1,2} C_{2k} + \text{h.c.}) + \sum_{\alpha, k} C_{\alpha k}^\dagger \Gamma_k^{(\alpha)} C_{\alpha k}, \quad (2)$$

with $C_{\alpha k}^\dagger = (c_{\alpha k\uparrow}^\dagger, c_{\alpha k\downarrow}^\dagger)$ the fermion operators, $\Gamma_k^{1,2} = 2(t^d + i\boldsymbol{\lambda} \cdot \boldsymbol{\sigma}) \cos(\frac{k_x}{2} + \frac{k_y}{2}) + 2(t^d - i\boldsymbol{\lambda} \cdot \boldsymbol{\sigma}) \cos(\frac{k_x}{2} - \frac{k_y}{2})$ the inter-sublattice couplings and $\Gamma_k^{(\alpha)} = (-1)^\alpha 2(t^x \cos k_x + t^y \cos k_y) + (\mu_\alpha + \mathbf{m}_\alpha \cdot \boldsymbol{\sigma})$ the intra-sublattice terms.

We firstly turn off the SOC by setting $\lambda^{d_1} = \lambda^{d_2} = 0$, then the system has a pure lattice point group symmetry $D_{2h} = \{E, C_2^z\} \times \{E, C_2^x\} \times \{E, \mathcal{I}\}$. In this case the $\Gamma_k^{1,2}$ term vanishes on the boundary of the BZ. In other words, the two species of fermions C_{1k} and C_{2k} do not hybridize if $k_x = \pi$ or $k_y = \pi$. It can be shown that on the C_2^x symmetric boundary line (k_x, π) , the C_{1k}, C_{2k} bands carry C_2^x quantum numbers 1, -1, respectively. Similarly, on the C_2^y symmetric line (π, k_y) the C_{1k}, C_{2k} bands carry C_2^y quantum numbers -1 and 1, respectively. Owing to these different quantum numbers, if the C_{1k} and C_{2k} bands are inverted, the band crossing will be protected from opening a gap. Resultantly, on the boundary lines (k_x, π) and/or (π, k_y) there will be pairs of Weyl cones (see Fig.1(b) as an example) among which the two in each pair are related by the inversion \mathcal{I} operation. It can be shown that the condition for the band crossings on the BZ boundaries is [see the Supplemental Materials (SM) for details] $-2(t^x + t^y) - |\mathbf{m}| \leq \mu_- \leq 2|t^y - t^x| + |\mathbf{m}|$, in which case the energy bands form a Weyl semimetal.

Now we turn on the SOC. If $\boldsymbol{\lambda} \cdot \mathbf{m} = 0$ is satisfied, then the Weyl cones remain massless. Otherwise, if $\boldsymbol{\lambda} \cdot \mathbf{m} \neq 0$ then all the Weyl cones obtain a mass and the energy band is fully gapped (see Fig.1(c)). Noticing that the SOC does not break the inversion symmetry \mathcal{I} , and that the pattern of the Berry curvature of the occupied bands is invariant under \mathcal{I} [see Fig.1(d), the small inversion anti-symmetric part of the Berry curvature is owing to the k -dependent unitary transformation], each pair of Weyl cones (related by \mathcal{I}) together contribute either 1 or -1 to the total Chern number (recalling that a single cone carries a π Berry phase or $\pm 1/2$ Chern number).

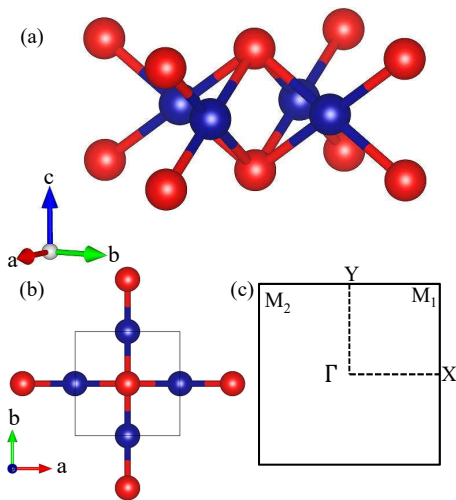


FIG. 2. Crystal structure of the monolayer CrO viewed along (a) [110] and (b) [001] directions. (c) The Brillouin zone and the corresponding high-symmetry points. The red and blue balls represent the O and Cr atoms, respectively.

Therefore, if there are an odd number of pairs of Weyl cones, the Chern number in the gapped state must be nonzero and the system will exhibit QAH effect.

Further analysis indicates that the total Chern number is equal to ± 1 under the following conditions,

$$t^d \neq 0, \quad \boldsymbol{\lambda} \cdot \mathbf{m} \neq 0, \quad (3)$$

$$\left| |\mathbf{m}| - 2|t^y - t^x| \right| < |\mu_-| < |\mathbf{m}| + 2|t^y - t^x|. \quad (4)$$

The above conditions can be satisfied in AFM materials with low point group symmetry (such as the monoclinic or triclinic systems). In later discussion we apply strain to lower the lattice symmetry.

Now we stress that the spin-orbit coupling term in model (1) is inversion symmetric. When $\boldsymbol{\lambda}^{d_1} = \lambda \hat{x}$, $\boldsymbol{\lambda}^{d_2} = \lambda \hat{y}$, it looks like a Rashba SOC term, but the difference is that the Rashba term breaks \mathcal{I} symmetry while our model (1) does not. In this case, the QAH effect can be realized if conditions $\mathbf{m} \cdot (\hat{x} + \hat{y}) \neq 0$ and (4) are satisfied.

It is interesting to compare the model (1) with the Haldane model[9] and the FM QAH model[10]. Without introducing external magnetic fields, all of these models have a gapped ground state with a nonzero Chern number. In the Haldane model, a staggered flux is needed in which the fermions obtain the Aharonov-Bohm phase. Although the total flux is zero, a staggered flux is not easy to implement in practice. In the FM QAH model, the staggered flux is replaced by the Berry phase resulting from spin-orbit coupling, and the role of the FM order is to polarize the spin of the electrons. However, the FM critical temperature in insulators is generally very low. In our model, the AFM order provides a local Zeeman field for the electrons, the SOC and the sub-lattice dependent chemical potentials guarantee a full gap and a nontrivial

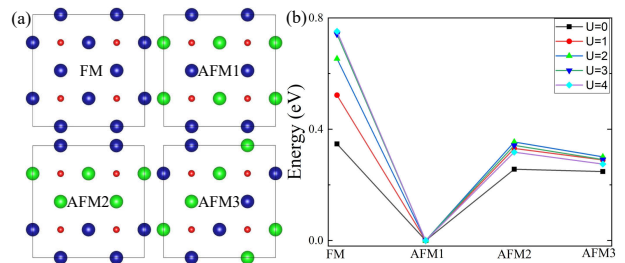


FIG. 3. (a) Cartoon pictures for four possible magnetic structures of a monolayer CrO, where FM and AFM represent ferromagnetism and antiferromagnetism, respectively. The blue and green balls represent Cr atoms with opposite spin. (b) The relative energies (per Cr atom) of the four ordered states under different Hubbard U (eV).

Chern number. The advantage is that the AFM critical temperature can be very high (even with an order of 1000 Kelvin). Therefore, if the band gap is not too small, then hopefully the QAH effect can be realized in experiments close to room temperatures.

As discussed above, the low-energy effective model (1) reveals the possibility that QAH effect can exist in AFM insulators. In the following, by studying a concrete material as a prototype — a monolayer CrO, we illustrate that QAH effect can indeed be obtained in AFM materials.

Candidate Material. A monolayer CrO has a square lattice structure whose symmetry is described by the symmorphic space group $P4\text{-mmm}$. The point group of $P4\text{-mmm}$ is D_{4h} generated by C_4^z, C_2^x and \mathcal{I} . The unit cell of a monolayer CrO contains two O atoms plus two Cr atoms (see Fig.2 (a) and (b)) and the corresponding BZ is shown in Fig.2 (c). The Cr^{2+} ions have a fairly strong correlation and they interact with each other via super-exchange interactions mediated by the O atoms. It was suggested in Ref.[30] that monolayer CrO is in antiferromagnetic phase with a high Neel temperature.

To confirm the magnetic structure of a monolayer CrO, we compare the energies of four trial states with different magnetic orders under different Hubbard U . As shown in Fig.3(a), indeed the AFM1 state (i.e. the collinear Neel state) is always lowest in energy. Notice that the AFM1 order has no ‘effective time-reversal symmetry’ like \mathcal{IT} or $\{\mathcal{T}|\tau\}$. Furthermore, since the electronic band structure is sensitive to the Hubbard U , we need to determine the proper value of U . By comparing the electronic band structure of Heyd-Scuseria-Ernzerhof (HSE) hybrid functional within the framework of HSE06[31], we find that $U = 3.2$ eV, which is slightly less than 3.5 eV as proposed in [30]. This is due to the fact that our relaxed lattice parameter is 1.4 percent less than that adopted in [30].

When ignoring the SOC, a monolayer CrO has a magnetic point group symmetry $4'/\text{mmm}'$ generated by $\mathcal{TC}_4^z, M_z, M_x$ and \mathcal{TM}_{xy} where all the rotation operations act on the lattice only. According to the \mathcal{TC}_2^{xy} sym-

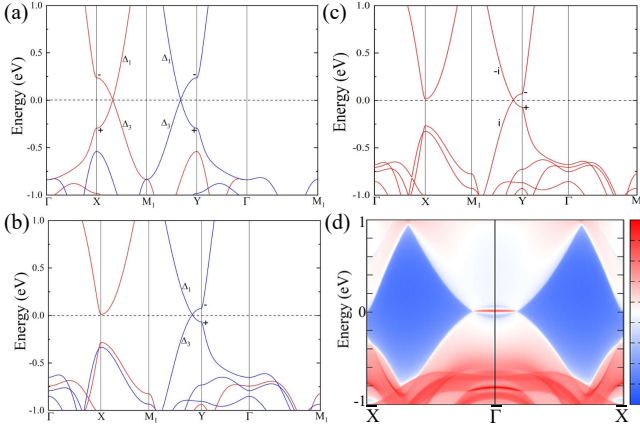


FIG. 4. The band structure of monolayer CrO along the high-symmetry directions, (a) no SOC, (b) no SOC, but tensile strain 10 percent along b direction, (c) with SOC, tensile strain 10 percent. The spin-up and spin-down bands in (a) and (b) are marked in red and blue, respectively. + and - represent parity quantum numbers, Δ_1 and Δ_3 represent different irreducible representations of C_{2v} point group, i and $-i$ are the eigenvalues of C_2^x under SOC. (d) Spectral function of monolayer CrO with semi-infinite Cr-O termination edge. The red-blue color scale represents the spectral density.

metry, the spin-up and spin-down are degenerate on the high-symmetry lines Γ - M_1 and Γ - M_2 . Away from these two high symmetry lines, the spin degeneracy is generally lifted as illustrated in Fig.4(a), where the red and blue lines represent spin-up and spin-down bands, respectively. Furthermore, the band inversion occurs around the X and Y points which are related to each other by the \mathcal{TC}_4^z symmetry and hence carry opposite spins. Since the two inverted bands carry different quantum numbers of C_{2v} , the band inversion results in a band crossing with two pairs of Weyl points[30]. The two pairs of Weyl cones around the X,Y points can also appear in the model (1) when $t^x = t^y$ and $\lambda = 0$.

If the \mathcal{TC}_4^z symmetry is preserved, then after the two pairs of Weyl cones being gapped out, the Berry curvature contributed from these cones will exactly cancel each other, resulting in a trivial Chern number. Therefore, in order to realize the QAH effect in a monolayer CrO, the \mathcal{TC}_4^z symmetry must be removed. To this end, we apply a tensile strain 10 percent along the b-direction. Then the point group symmetry of monolayer CrO reduces to D_{2h} , which is generated by C_2^z , C_2^x and \mathcal{I} .

Under the above tensile strain, the calculated electronic band structure is shown in Fig.4(b), where the pair of Weyl points on the X- M_1 axis merge and gap out with the disappearing of band inversion. But the pair of Weyl points on the Y- M_1 axis still remain. When considering the SOC, our calculations indicate that the magnetic moments lie in the lattice plane. We assume that the magnetic moments are along the x -direction, then the monolayer CrO has a magnetic point group symme-

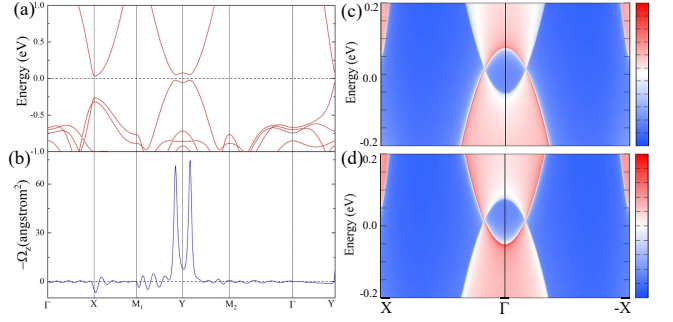


FIG. 5. (a) The electronic band structure of monolayer CrO with SOC when breaking the C_2^x symmetry. (b) The Berry curvature of monolayer CrO when breaking the C_2^x symmetry. The spectral function of monolayer CrO with a semi-infinite (c) Cr and (d) Cr-O termination edge when breaking the C_2^x symmetry. The red-blue color scale represents the spectral density.

try $2'/m'm$ generated by \mathcal{TC}_2^z , \mathcal{TM}^z and M_x . With the SOC, the electronic band structure of a monolayer CrO with the tensile strain is shown in Fig.4(c), where the pair of Weyl points on the Y- M_1 line are still present owing to the protection of the spin-orbit coupled C_2^x symmetry.

Now we obtain a single pair of Weyl cones which are inversion partner of each other. The spatial inversion symmetry ensures that the Berry curvature around the two cones are equal. Interestingly, like the existence of fermi arc linking two Weyl cones in 3D, we also find fermi-arc like zero-energy edge modes which links the two Weyl cones, as shown in Fig.4(d). In the SM, we show that the existence of the fermi-arc like zero energy modes are protected by the nontrivial 1D winding number for momentum points linking the two cones.

If the cones are gapped out, the preserved inversion symmetry guarantees that the total Chern number is nonzero. Accordingly, we need to further break the C_2^x symmetry. This can be achieved by adding a shear strain, e.g., by changing the angle between the a-axis and the b-axis from 90° to 88° . The resultant symmetry group is $2'/m' = \{E, \mathcal{I}, \mathcal{TC}_2^z, \mathcal{TM}_z\}$. Due to the reduction of symmetry, the Weyl cones on the Y- M_1 axis finally open a gap, as shown in Fig.5 (a). The resultant gapped ground state has a Chern number $C = -1$, which makes the strained monolayer CrO be a QAH insulator. As shown in Fig.5(b), the Berry curvature mainly concentrates around the gapped Weyl points. Finally, the appearance of QAH effect is further confirmed by the presence of topologically protected chiral edge states, as shown in Fig.5(c) and (d).

The Neel temperature of a monolayer CrO is estimated to be above the room temperature[30]. Our calculations indicate that the combination of tensile and shear strain drives monolayer CrO into a Chern insulator with a band gap of order of 100 Kelvin. Thus it is expected that the temperature for observing the QAH effect will be greatly

enhanced (for about two orders of magnitude higher) compared to that in the ferromagnets. This is a very exciting result. We believe that it will arouse further interest in the study of QAH effect in AFM systems, and that the critical temperature of the QAH phase can be further increased.

In summary, we come up with a four-band lattice model to illustrate that QAH effect can exist in antiferromagnetism. Furthermore, we predict that the monolayer CrO is a candidate AFM material to realize the QAH effect. Based on symmetry analysis and the first-principles electronic structure calculations, we first show that a monolayer CrO is an AFM semimetal containing Weyl cones which are robust against SOC. Then we demonstrate that by adding tensile and shear strain, the monolayer CrO can be turned into an AFM QAH insulator. Our study reveals a new scenario to realize QAH insulator in AFM materials. Especially, once QAH insulator is realized in AFM systems, it may allow people to observe QAH effect close to room temperatures.

Methods. The electronic structures of a monolayer CrO were studied with the projector augmented wave method[32, 33] as implemented in the VASP package[34, 35]. The Perdew-Burke-Ernzerhof exchange-correlation functional at the generalized gradient approximation level was adopted to describe the interaction between the ionic cores and the valence electrons[36]. For the electronic correlation in the d orbitals of Cr^{2+} , we adopted the Hubbard U formalism. The kinetic energy cutoff of the plane-wave basis was set to 700 eV and a $20 \times 20 \times 1$ was adopted for the k -point mesh. The Gaussian smearing method with a width of 0.01 eV was utilized for the Fermi surface broadening. Both cell parameters and internal atomic positions were fully relaxed until the forces on all atoms were smaller than 0.001 eV/Å. The calculated lattice parameters were 1.4 percent less than the previous values[30]. A 20 Å vacuum layer was used to avoid the residual interaction between adjacent layers. The Berry curvature of monolayer CrO was calculated by using the Wannier90 package[37, 38]. The topological invariants and the chiral edge states of monolayer CrO were studied by WannierTools package[39].

Acknowledgments. We thank X.-H. Kong, Z.-M. Yu for helpful discussions. This work was financially supported by the NSF of China (No. 12134020, No. 11974421 and No. 11934020).

* guopengjie@ruc.edu.cn

† liuzxphys@ruc.edu.cn

‡ zlu@ruc.edu.cn

- [1] T. Jungwirth, Q. Niu, and A. H. MacDonald, Anomalous hall effect in ferromagnetic semiconductors, *Phys. Rev. Lett.* **88**, 207208 (2002).
 [2] N. Nagaosa, J. Sinova, S. Onoda, A. H. MacDonald, and

- N. P. Ong, Anomalous hall effect, *Rev. Mod. Phys.* **82**, 1539 (2010).
 [3] H. Weng, R. Yu, X. Hu, X. Dai, and Z. Fang, Quantum anomalous hall effect and related topological electronic states, *Advances in Physics* **64**, 227 (2015), <https://doi.org/10.1080/00018732.2015.1068524>.
 [4] C.-X. Liu, S.-C. Zhang, and X.-L. Qi, The quantum anomalous hall effect: Theory and experiment, *Annual Review of Condensed Matter Physics* **7**, 301 (2016), <https://doi.org/10.1146/annurev-conmatphys-031115-011417>.
 [5] C.-Z. Chang and M. Li, *J. Phys.: Condens. Matter* **28**, 123002 (2016).
 [6] K. He, Y. Wang, and Q.-K. Xue, Topological materials: Quantum anomalous hall system, *Annual Review of Condensed Matter Physics* **9**, 329 (2018), <https://doi.org/10.1146/annurev-conmatphys-033117-054144>.
 [7] Y. Tokura, K. Yasuda, and A. Tsukazaki, Magnetic topological insulators, *Nature Reviews Physics* **1**, 126 (2019).
 [8] C.-Z. Chang, C.-X. Liu, and A. H. MacDonald, *ArXiv: 2202*, 13902 (2022).
 [9] F. D. M. Haldane, Model for a quantum hall effect without landau levels: Condensed-matter realization of the "parity anomaly", *Phys. Rev. Lett.* **61**, 2015 (1988).
 [10] X.-L. Qi, Y.-S. Wu, and S.-C. Zhang, Topological quantization of the spin hall effect in two-dimensional paramagnetic semiconductors, *Phys. Rev. B* **74**, 085308 (2006).
 [11] C.-X. Liu, X.-L. Qi, X. Dai, Z. Fang, and S.-C. Zhang, Quantum anomalous hall effect in $\text{Hg}_{1-y}\text{Mn}_y\text{Te}$ quantum wells, *Phys. Rev. Lett.* **101**, 146802 (2008).
 [12] R. Yu, W. Zhang, H.-J. Zhang, S.-C. Zhang, X. Dai, and Z. Fang, Quantized anomalous hall effect in magnetic topological insulators, *Science* **329**, 61 (2010).
 [13] Z. F. Wang, Z. Liu, and F. Liu, Quantum anomalous hall effect in 2d organic topological insulators, *Phys. Rev. Lett.* **110**, 196801 (2013).
 [14] C. Fang, M. J. Gilbert, and B. A. Bernevig, Large- Chern-number quantum anomalous hall effect in thin-film topological crystalline insulators, *Phys. Rev. Lett.* **112**, 046801 (2014).
 [15] S.-C. Wu, G. Shan, and B. Yan, Prediction of near-room-temperature quantum anomalous hall effect on honeycomb materials, *Phys. Rev. Lett.* **113**, 256401 (2014).
 [16] Y. Ren, J. Zeng, X. Deng, F. Yang, H. Pan, and Z. Qiao, Quantum anomalous hall effect in atomic crystal layers from in-plane magnetization, *Phys. Rev. B* **94**, 085411 (2016).
 [17] C. Huang, J. Zhou, H. Wu, K. Deng, P. Jena, and E. Kan, Quantum anomalous hall effect in ferromagnetic transition metal halides, *Phys. Rev. B* **95**, 045113 (2017).
 [18] P. Chen, J.-Y. Zou, and B.-G. Liu, Intrinsic ferromagnetism and quantum anomalous hall effect in a CoBr_2 monolayer, *Phys. Chem. Chem. Phys.* **19**, 13432 (2017).
 [19] J.-Y. You, Z. Zhang, B. Gu, and G. Su, Two-dimensional room-temperature ferromagnetic semiconductors with quantum anomalous hall effect, *Phys. Rev. Applied* **12**, 024063 (2019).
 [20] F. Wu, T. Lovorn, E. Tutuc, I. Martin, and A. H. MacDonald, Topological insulators in twisted transition metal dichalcogenide homobilayers, *Phys. Rev. Lett.* **122**, 086402 (2019).
 [21] D. Zhang, M. Shi, T. Zhu, D. Xing, H. Zhang, and J. Wang, Topological axion states in the magnetic insu-

- lator mnbi_2te_4 with the quantized magnetoelectric effect, *Phys. Rev. Lett.* **122**, 206401 (2019).
- [22] Y.-H. Zhang, D. Mao, and T. Senthil, Twisted bilayer graphene aligned with hexagonal boron nitride: Anomalous hall effect and a lattice model, *Phys. Rev. Research* **1**, 033126 (2019).
- [23] Y.-H. Zhang, D. Mao, Y. Cao, P. Jarillo-Herrero, and T. Senthil, Nearly flat chern bands in moiré superlattices, *Phys. Rev. B* **99**, 075127 (2019).
- [24] N. Bultinck, S. Chatterjee, and M. P. Zaletel, Mechanism for anomalous hall ferromagnetism in twisted bilayer graphene, *Phys. Rev. Lett.* **124**, 166601 (2020).
- [25] J. Shi, J. Zhu, and A. H. MacDonald, Moiré commensurability and the quantum anomalous hall effect in twisted bilayer graphene on hexagonal boron nitride, *Phys. Rev. B* **103**, 075122 (2021).
- [26] C.-Z. Chang, J. Zhang, X. Feng, J. Shen, Z. Zhang, M. Guo, K. Li, Y. Ou, P. Wei, L.-L. Wang, Z.-Q. Ji, Y. Feng, S. Ji, X. Chen, J. Jia, X. Dai, Z. Fang, S.-C. Zhang, K. He, Y. Wang, L. Lu, X.-C. Ma, and Q.-K. Xue, Experimental observation of the quantum anomalous hall effect in a magnetic topological insulator, *Science* **340**, 167 (2013).
- [27] Y. Deng, Y. Yu, M. Z. Shi, Z. Guo, Z. Xu, J. Wang, X. H. Chen, and Y. Zhang, Quantum anomalous hall effect in intrinsic magnetic topological insulator mnbi_2te_4 , *Science* **367**, 895 (2020).
- [28] M. Serlin, C. L. Tschirhart, H. Polshyn, Y. Zhang, J. Zhu, K. Watanabe, T. Taniguchi, L. Balents, and A. F. Young, Intrinsic quantized anomalous hall effect in a moiré heterostructure, *Science* **367**, 900 (2020).
- [29] T. Li, S. Jiang, B. Shen, Y. Zhang, L. Li, Z. Tao, T. Devakul, K. Watanabe, T. Taniguchi, L. Fu, J. Shan, and K. F. Mak, Quantum anomalous hall effect from inter-twined moiré bands, *Nature* **600**, 641 (2021).
- [30] X. Chen, D. Wang, L. Li, and B. S. Sanyal, ArXiv: **2104**, 07390 (2021).
- [31] A. F. Izmaylov, E. N. Brothers, and G. E. Scuseria, Linear-scaling calculation of static and dynamic polarizabilities in hartree-fock and density functional theory for periodic systems, *The Journal of Chemical Physics* **125**, 224105 (2006), <https://doi.org/10.1063/1.2404667>.
- [32] P. E. Blöchl, Projector augmented-wave method, *Phys. Rev. B* **50**, 17953 (1994).
- [33] G. Kresse and D. Joubert, From ultrasoft pseudopotentials to the projector augmented-wave method, *Phys. Rev. B* **59**, 1758 (1999).
- [34] G. Kresse and J. Furthmüller, Efficiency of ab-initio total energy calculations for metals and semiconductors using a plane-wave basis set, *Computational Materials Science* **6**, 15 (1996).
- [35] G. Kresse and J. Furthmüller, Efficient iterative schemes for ab initio total-energy calculations using a plane-wave basis set, *Phys. Rev. B* **54**, 11169 (1996).
- [36] J. P. Perdew, K. Burke, and M. Ernzerhof, Generalized gradient approximation made simple, *Phys. Rev. Lett.* **77**, 3865 (1996).
- [37] N. Marzari and D. Vanderbilt, Maximally localized generalized wannier functions for composite energy bands, *Phys. Rev. B* **56**, 12847 (1997).
- [38] I. Souza, N. Marzari, and D. Vanderbilt, Maximally localized wannier functions for entangled energy bands, *Phys. Rev. B* **65**, 035109 (2001).
- [39] Q. Wu, S. Zhang, H.-F. Song, M. Troyer, and A. A. Soluyanov, Wanniertools: An open-source software package for novel topological materials, *Computer Physics Communications* **224**, 405 (2018).